Tracer Studies of High-Shear Granulation: II. Population Balance Modeling

M. J. Hounslow
Particle Products Group, Dept. of Chemical and Process Engineering, University of Sheffield, Sheffield, U.K.

J. M. K. Pearson
Dept. of Chemical Engineering, University of Cambridge, Cambridge, U.K.

T. Instone
Unilever Research, Port Sunlight Laboratory, U.K.

A population balance framework developed describes the tracer studies in Part I. A two internal coordinate population balance equation (PBE) links the evolution with time of granule-size and tracer-mass distributions to underlying rate processes. A new analytical PBE was developed for the tracer distribution and novel numerical techniques, including a new discretized population balance equation for breakage or grinding. Also developed is a general differential technique for extracting rate constants from measurements of particle-size distributions. Granulation in a high-shear mixer proceeds after nucleation, not studied here, with very high initial breakage rates but a relatively unchanging aggregation rate constant. The breakage function is bimodal on a mass basis and the selection rate decays exponentially over about 20 s. A heterogeneous strength hypothesis was used to account for this time dependence. Aggregation rates are the highest for interactions between small and large granules and may be quantitatively given by the Equipartition of kinetic energy kernel developed from the theory of collisions between gas molecules. The model can describe granule-size and tracer-mass distributions simultaneously with great accuracy. The need to replace time as a driving force variable in the kinetics for these systems is identified.

Introduction

In Part I of this series we described how we explored the mechanisms active during high-shear granulation by adding spikes of tracer granules to a batch granulator. The purpose of the current article is to develop quantitative methods for extracting rates and kinetics of the active processes from the tracer and size distribution data.

Population balance equations (PBEs) are widely used in many branches of science and engineering to relate observed distributions of properties to the rates of the underlying process that changes those distributions (Hulburt and Katz, 1964; Ramkrishna, 1985; Randolph and Larson, 1988; Hounslow, 1998).

PBEs have been used in granulation studies for many years (Sastry, 1975; Adetayo et al., 1995). Generally, their purpose has been to reduce a mass of experimental data to a simple, often empirical, rate constant. This might allow some interpretation of the underlying physics, but is perhaps best used as a way of modeling for design or control purposes.

In the work reported here, we wish to get much closer to the underlying physics of the problem. We are able to do so because we have data not just in one dimension (that of granule size), but as a projection from another, that of tracer content. The fact that we can add tracer in narrow size ranges allows us to investigate the effect of granule size in a manner decoupled from time or granule age. As we have previously reported (Pearson et al., 1998), this decoupling of age size is essential if model discrimination is to be attempted.

Theory

If granules are described by only one property (or internal coordinate as Hulburt and Katz have it), their size, here identified as v, then a quite general PBE for a well-mixed

Correspondence concerning this article should be addressed to M. J. Hounslow.

closed region is

$$\frac{\partial n(t,v)}{\partial t} = B^0(t,v) \qquad \text{Nucleation or source term}$$

$$-\frac{\partial}{\partial v}[G(t,v)n(t,v)] \qquad \text{Growth term}$$

$$+\frac{1}{2}\int_0^v \beta(t,v-\epsilon,\epsilon)n(t,v-\epsilon)n(t,\epsilon)d\epsilon$$

$$-n(t,v)\int_0^\infty \beta(t,v,\epsilon)n(t,\epsilon)d\epsilon \qquad \text{Aggregation term}$$

$$+\int_v^\infty S(t,\epsilon)b(v,\epsilon)n(t,\epsilon)d\epsilon - S(t,v)n(t,v) \qquad \text{Breakage term}$$

$$-O(t,v)n(t,v) \qquad \text{Sink term}$$

In this article we seek a form of the previous equation appropriate for modeling the granule-size distributions (GSD) from high-shear granulation experiments and an analogous expression for modeling the tracer-mass distributions (TMDs).

In this section we develop three PBEs in which granules are first represented in a two-dimensional (2-D) space: every granule has two properties, or internal coordinates, which completely specify their behavior, that is, size and tracer content. The second PBE describes the GSD and the third, the TMD. The PBEs are first deduced in analytical form as partial differential integral equations and then presented in a discretized form as ordinary differential equations suitable for solution by computer.

In Part I of this series of articles (Pearson et al., 2001), we identify the mechanisms, or processes, active during our high-shear granulation experiments as being aggregation and breakage. In Eq. 1 the rates of these processes are described by an aggregation rate constant, or kernel β, a selection rate constant S, and a breakage function b. The aggregation rate constant is the constant of proportionality relating the rate of formation of aggregates to the product of concentrations of the two kinds of granules interacting to form the new aggregate, in much the same way as a second-order reaction rate constant in chemical kinetics. In this way, we implicitly assume that aggregation events are binary but allow that granules of differing internal coordinates may have different rate constants. The selection rate constant is the constant of proportionality between the rate of selection of granules for breakage and their concentration, this time in direct analogy with a first-order reaction rate constant. The breakage function is the distribution of fragment sizes observed when granules of a particular type are selected.

Analytical forms

We allow that every granule has two distinct properties, that is, size, measured by granule mass v (we clearly foreshadow here that we will in due course make an assumption of constant density and replace particle mass with particle volume), and tracer content measured by mass of tracer c. The 2-D probability density function $f(t,v,c)$ gives the number of granules with $v \in (v, v+dv)$ and $c \in (c, c+dc)$ as $dN = f(t,v,c)dvdc$. The conventional number density distribution $n(t,v)$, which gives the number of granules with $v \in (v, v+dv)$ as $dN = n(t,v)dv$, may be obtained from f by integrating over all possible tracer masses ($0 \le c \le v$)

$$n(t,v) = \int_0^v f(t,v,c)dc \tag{2}$$

In this way we see that n is the zeroth moment of f with respect to tracer mass. The first moment of f with respect to tracer mass is the tracer-mass density function $M(t,v)$, which relates the mass of tracer contained within granules in the *size* range $v \in (v, v+dv)$ as

$$M(t,v) = \int_0^v cf(t,v,c)dc \tag{3}$$

It is worth noting that while f is very difficult to measure (to do so would require either an instrument capable of measuring v and c simultaneously, or to take the measurement by hand of each of these quantities for one granule at a time); n and M can be measured relatively easily, as indeed we report in Part I of this series.

In this work we normalize the density functions to refer to 1 kg of granules and usually report them with a linear dimension l as the internal coordinate. In this way $n(t,l)$ has units of $\mathrm{kg}^{-1}\cdot\mathrm{m}^{-1}$ and $M(t,l)$ m^{-1}. This normalization results in the third moment of n, taking on a value of $m_3 = 1/(\rho_s k_v) = 7.64\times10^{-4}$ $\mathrm{m}^3\cdot\mathrm{kg}^{-1}$. The mass density function, $w(t,l) = \rho_s k_v l^3 n(t,l)$ then normalizes to a value of 1.

2-D Population Balance Equation. The PBE with aggregation and breakage active is

$$\frac{\partial f}{\partial t} = (B^A - D^A) + (B^B - D^B) \tag{4}$$

The rate of birth by aggregation is

$$B^A(t,v,c) = \frac{1}{2}\int_0^v \int_0^{\min(c,v-\epsilon)} \beta(t,v-\epsilon,\epsilon)f(t,v-\epsilon,c-\gamma) \times f(t,\epsilon,\gamma)d\gamma d\epsilon \tag{5}$$

wherein we have allowed that the aggregation rate constant depends on time, and the size of both granules (v and $v-\epsilon$), but not the tracer content of either granule. The associated death rate is

$$D^A(t,v,c) = f(t,v,c)\int_0^\infty \int_0^\epsilon \beta(t,v,\epsilon)f(t,\epsilon,\gamma)d\gamma d\epsilon \tag{6}$$

While we may also assume with confidence that the selection rate constant does not depend on tracer content, the breakage function requires rather more careful consideration. The breakage function relates the probability of forming fragments of size v containing tracer c from granules of size ϵ containing tracer γ; that is, b has five arguments $b(t,v,c,\epsilon,\gamma,)$. In all of the work presented here, we neglect the effect of time and assume that the fraction, or concentration, of tracer in the fragment is the same as in the original granule, that is, $\gamma/\epsilon = c/v$. The tracer-dependence of b can

now be separated from the size dependence as

$$b(v,c,\epsilon,\gamma) = b(v,\epsilon)\delta(c - v\gamma/\epsilon) \tag{7}$$

If follows that the breakage birth term is

$$\begin{aligned} B^B(t,v,c) &= \int_v^\infty \int_c^\epsilon S(t,\epsilon) b(v,c,\epsilon,\gamma) f(t,\epsilon,\gamma) d\gamma d\epsilon \\ &= \int_v^\infty S(t,\epsilon) b(v,\epsilon) f(t,\epsilon,\epsilon c/v) \frac{\epsilon}{v} d\epsilon \end{aligned} \tag{8}$$

The associated death term is

$$D^B(t,v,c) = S(t,v) f(t,v,c) \tag{9}$$

1-D Population Balance Equation for the GSD. Noting the relationship between f and n in Eq. 2 and applying the implied integrating to Eq. 4 yields

$$\frac{\partial n(t,v)}{\partial t} = \left(\overline{B}_0^A - \overline{D}_0^A\right) + \left(\overline{B}_0^B - \overline{D}_0^B\right) \tag{10}$$

where the subscript 0 denotes that the indicated terms are zeroth moments of the originals.

Integration of the aggregation birth term yields

$$\begin{aligned} \overline{B}_0^A(t,v) &= \int_0^v B^A(t,v,c) dc \\ &= \frac{1}{2}\int_0^v \int_0^v \int_0^{\min(c,v-\epsilon)} \beta(t,v-\epsilon,\epsilon) \\ &\quad \times f(t,v-\epsilon,c-\gamma) f(t,\epsilon,\gamma) d\gamma d\epsilon dc \\ &= \frac{1}{2}\int_0^v \beta(t,v-\epsilon,\epsilon) \int_0^\epsilon f(t,\epsilon,\gamma) \int_0^{v-\epsilon} \\ &\quad \times f(t,v-\epsilon,c-\gamma) d(c-\gamma) d\gamma d\epsilon \\ &= \frac{1}{2}\int_0^v \beta(t,v-\epsilon,\epsilon) n(t,\epsilon) n(t,v-\epsilon) d\epsilon \end{aligned} \tag{11}$$

which is, of course, the standard result of the 1-D PBE, Eq. 1. Integration of the death term gives, as expected

$$\overline{D}_0^A(t,v) = n(t,v) \int_0^\infty \beta(t,v,\epsilon) n(t,\epsilon) d\epsilon \tag{12}$$

Similar integration of the breakage terms gives

$$\begin{aligned} \overline{B}_0^B(t,v) &= \int_0^v \int_v^\infty S(t,\epsilon) b(v,\epsilon) f(t,\epsilon,\epsilon c/v) \frac{\epsilon}{v} d\epsilon dc \\ &= \int_v^\infty S(t,\epsilon) b(v,\epsilon) \int_0^\epsilon f(t,\epsilon,\epsilon c/v) d\left(\frac{\epsilon c}{v}\right) d\epsilon \\ &= \int_v^\infty S(t,\epsilon) b(v,\epsilon) n(t,\epsilon) d\epsilon \end{aligned} \tag{13}$$

and

$$\overline{D}_0^B(t,v) = S(t,v) n(t,v) \tag{14}$$

That Eqs. 11 to 14 should yield those well-known from simple 1-D PBEs is reassurance that the original equations, Eqs. 5 to 9, were correctly posed.

1-D Population Balance Equation for the TMD. The motivation for developing the 2-D PBE (Eq. 4) was that it provides a common basis from which to develop granule and tracer-mass distributions. The second part of that objective is now addressed. Proceeding as before: multiplication of Eq. 4 by c and integrating yields

$$\frac{\partial M(t,v)}{\partial t} = \left(\overline{B}_1^A - \overline{D}_1^A\right) + \left(\overline{B}_1^B - \overline{D}_1^B\right) \tag{15}$$

where the subscript 1 now denotes that the indicated terms are *first* moments of the originals.

Integration of the aggregation birth term yields

$$\begin{aligned} \overline{B}_1^A(t,v) &= \int_0^v c B^A(t,v,c) dc \\ &= \frac{1}{2}\int_0^v c \iint \beta(t,v-\epsilon,\epsilon) f(t,v-\epsilon,c-\gamma) f(t,\epsilon,\gamma) \\ &\quad \times d\gamma d\epsilon dc \\ &= \frac{1}{2}\int_0^v \beta(t,v-\epsilon,\epsilon) \iint [(c-\gamma)+\gamma] f(t,v-\epsilon,c-\gamma) \\ &\quad \times f(t,\epsilon,\gamma) d(c-\gamma) d\gamma d\epsilon \\ &= \frac{1}{2}\int_0^v \beta(t,v-\epsilon,\epsilon) \int f(t,\epsilon,\gamma) \int [(c-\gamma)+\gamma] \\ &\quad \times f(t,v-\epsilon,c-\gamma) d(c-\gamma) d\gamma d\epsilon \\ &= \frac{1}{2}\int_0^v \beta(t,v-\epsilon,\epsilon) \int f(t,\epsilon,\gamma) [M(t,v-\epsilon) \\ &\quad + \gamma n(t,v-\epsilon)] d\gamma d\epsilon \\ &= \frac{1}{2}\int_0^v \beta(t,v-\epsilon,\epsilon) [n(t,v) M(t,v-\epsilon) \\ &\quad + M(t,v) n(t,v-\epsilon)] d\epsilon \\ &= \int_0^v \beta(t,v-\epsilon,\epsilon) n(t,v) M(t,v-\epsilon) d\epsilon \end{aligned} \tag{16}$$

Similarly,

$$\overline{D}_1^A(t,v) = M(t,v) \int_0^\infty \beta(t,v,\epsilon) n(t,\epsilon) d\epsilon \tag{17}$$

$$\begin{aligned} \overline{B}_1^B(t,v) &= \int_0^v c \int_v^\infty S(t,\epsilon)\, b(v,\epsilon) f(t,\epsilon,\epsilon c/v) \frac{\epsilon}{v} d\epsilon dc \\ &= \int_v^\infty S(t,\epsilon) b(v,\epsilon) \int_0^\epsilon c f(t,\epsilon,\epsilon c/v) d\left(\frac{\epsilon c}{v}\right) d\epsilon \\ &= \int_v^\infty S(t,\epsilon) b(v,\epsilon) \frac{v}{\epsilon} M(t,\epsilon) d\epsilon \end{aligned} \tag{18}$$

$$\overline{D}_1^B(t,v) = S(t,v) M(t,v) \tag{19}$$

One of the important properties of these PBEs is that they correctly predict conservation of granule and tracer mass. The former is a routine property of the 1-D PBE for the GSD; the latter is demonstrated to be true in Appendix A provided that mass is conserved by breakage, that is

$$\epsilon = \int_0^\epsilon v b(v,\epsilon) dv \text{ or } \lambda^3 = \int_0^\lambda l^3 b(l,\lambda) dl \tag{20}$$

In principle it is now possible to solve Eqs. 10 and 15 simultaneously to obtain $n(t,v)$ and $M(t,v)$. However, as is usually the case with population balance problems, specialized numerical methods are required.

Numerical forms

In this section we develop discretized population balance equations (DPBEs) for the solution of Eqs. 10 and 15. The approach adopted is that the GSD and TMD are represented not by their density functions n and M, but by discrete amounts of material N_i and M_i, which are, respectively, the number of granules and the mass of tracer contained in granules, in the size range (l_i, l_{i+1}), that is

$$N_i(t) = \int_{l_i}^{l_{i+1}} n(t,l)\,dl \tag{21}$$

$$M_i(t) = \int_{l_i}^{l_{i+1}} M(t,l)\,dl \tag{22}$$

In all the work presented here the size intervals are arranged in a geometric series such that $l_{i+1}/l_i = \sqrt[3]{2}$.

Discretized Population Balance Equation for the GSD. The DPBE is

$$\frac{dN_i}{dt} = B^A_{0,i}(t) - D^A_{0,i}(t) + B^B_{0,i}(t) - D^B_{0,i}(t) \tag{23}$$

We use the aggregation terms developed by Hounslow et al. (1988)

$$B^A_{0,i}(t) - D^A_{0,i}(t) = N_{i-1}\sum_{j=1}^{i-2} 2^{j-i+1}\beta_{i-1,j}N_j + \frac{1}{2}\beta_{i-1,i-1}N_{i-1}^2 - N_i\sum_{j=1}^{i-1} 2^{j-i}\beta_{i,j}N_j - N_i\sum_{j=i}^{n_{eq}}\beta_{i,j}N_j \tag{24}$$

For breakage, we adapt the approach of Eyre et al. (1998). We seek to write

$$B^B_i - D^B_i = -S_iN_i + \sum_{j=i}^{n_{eq}} b_{i,j}S_jN_j \tag{25}$$

where S_i is the selection rate for interval i and $b_{i,j}$ is the number of fragments from interval j that are assigned to interval i. These functions are to be deduced from their continuous analog in a way that does not depend on the instantaneous size distribution (n or N_i). This is achieved by comparing rates of changes of total numbers and volumes and then assuming that n does not vary significantly across an interval.

Define the average number of fragments produced by breaking granules of size l as

$$N_b(t,l) = \int_0^l b(x,l)\,dx \tag{26}$$

The overall rate of generation of numbers is then

$$R_0(t) = \int_0^\infty \overline{B}^B_0(t,l) - \overline{D}^B_0(t,l)\,dl = \int_0^\infty \left[N_b(t,l) - 1\right]S(t,l)n(t,l)\,dl \tag{27}$$

The discrete equivalent of Eq. 27 is

$$\begin{aligned} R_0(t) &= \sum_i \left(B^B_i - D^B_i\right) \\ &= \sum_i \left(-S_iN_i + \sum_{j\ge i} b_{i,j}S_jN_j\right) \\ &= \left(-\sum_i S_iN_i\right) + \left(\sum_j \sum_{i\le j} b_{i,j}S_jN_j\right) \\ &= \left(-\sum_i S_iN_i\right) + \left(\sum_i \sum_{j\le i} b_{j,i}S_iN_i\right) \\ &= \sum_i S_iN_i\left(\left(\sum_{j\le i} b_{j,i}\right) - 1\right) \end{aligned} \tag{28}$$

For these last two results to be the same, the following must be true

$$\int_{l_i}^{l_{i+1}} \left[N_b(t,l) - 1\right]S(t,l)n(t,l)\,dl = S_iN_i\left[\left(\sum_{j\le i} b_{j,i}\right) - 1\right] \tag{29}$$

In order to use this result, some simple relationship between n and N is required. The simplest that might be used is

$$n(l) = \frac{N_i}{l_{i+1} - l_i} \qquad l_i \le l < l_{i+1} \tag{30}$$

Equation 29 then yields

$$S_i = \frac{\dfrac{1}{l_{i+1} - l_i}\displaystyle\int_{l_i}^{l_{i+1}} \left[N_b(t,l) - 1\right]S(t,l)\,dl}{\left(\displaystyle\sum_{j\le i} b_{j,i}\right) - 1} \tag{31}$$

In order to develop equations for $b_{i,j}$, we consider the movement of granule volume from one interval to another. The rate of generation of volume of fragments from interval i is

$$\int_{l_i}^{l_{i+1}} l^3S(t,l)n(t,l)\,dl \tag{32}$$

These fragments arrive in interval j at a rate

$$\begin{aligned} &\int_{l_i}^{l_{i+1}}\int_{l_j}^{l_{j+1}} x^3S(t,l)n(t,l)b(x,l)\,dx\,dl \qquad j < i \\ &\int_{l_i}^{l_{i+1}}\int_{l_i}^{l} x^3S(t,l)n(t,l)b(x,l)\,dx\,dl \qquad j = i \end{aligned} \tag{33}$$

The discrete equivalents of Eqs. 32 and 33 are $\bar{l}_i^3N_iS_i$ and $l_l^3b_{j,i}N_iS_i$, respectively. It follows that volume will be appor-

tioned appropriately to the intervals if

$$\left.\begin{aligned}\left(\frac{\bar{l}_j}{\bar{l}_i}\right)^3 b_{j,i} &= \frac{\int_{l_i}^{l_{i+1}}\int_{l_j}^{l_{j+1}} x^3 S(t,l) n(t,l) b(x,l)\,dx\,dl}{\int_{l_i}^{l_{i+1}} l^3 S(t,l) n(t,l)\,dl} \approx \frac{\int_{l_i}^{l_{i+1}}\int_{l_j}^{l_{j+1}} x^3 S(t,l) b(x,l)\,dx\,dl}{\int_{l_i}^{l_{i+1}} l^3 S(t,l)\,dl} \\ \text{and } b_{i,i} &\approx \frac{\int_{l_i}^{l_{i+1}}\int_{l_j}^{l} x^3 S(t,l) b(x,l)\,dx\,dl}{\int_{l_i}^{l_{i+1}} l^3 S(t,l)\,dl}\end{aligned}\right\} \tag{34}$$

Together Eqs. 25, 31, and 34 provide a DPBE for breakage. In Appendix B it is demonstrated that this formulation has the property that granule volume *must* be conserved.

Testing the breakage DPBE. While Eq. 24 has been often used and tested, Eqs. 31 and 34 are new. As a demonstration of their accuracy, we will now consider a breakage-only problem for which there is an *analytical* solution. We take the selection rate to increase simply with size cubed and choose the binary breakage function that gives uniform probability of all fragment sizes on a volume scale ($b(\epsilon, v) = 1/v$) that is

$$S(t,l) = l^3 \quad \text{and} \quad b(x,l) = \frac{6x^2}{l^3}$$

If the initial condition is $n(0,l) = 3l^2 e^{-l^3}$, the *analytical* solution for this problem is

$$n(t,l) = 3l^2(1+t)^2 e^{-l^3(1+t)} \tag{35}$$

The *numerical* solution is obtained as follows

Equation 34 gives

$$\left.\begin{aligned} b_{j,i} &= \left(\frac{\bar{l}_i}{l_j}\right)^3 \frac{\int_{l_i}^{l_{i+1}}\int_{l_j}^{l_j} x^3 l^3 6x^2/l^3\,dx\,dl}{\int_{l_i}^{l_{i+1}} l^3 l^3\,dl} = \left(\frac{\bar{l}_i}{\bar{l}_j}\right)^3 \frac{(l_{i+1}-l_i)\left(l_{j+1}^6 - l_j^6\right)}{\frac{1}{7}\left(l_{i+1}^7 - l_i^7\right)} \\ &= r^{3(j-i)} \frac{7r(r-1)(r^6-1)}{r^7-1} = 1.35118 \times 2^{j-i} \\ \text{and } b_{i,i} &= \frac{\int_{l_i}^{l_{i+1}}\int_{l_j}^{l} x^3 l^3 6x^2/l^3\,dx\,dl}{\int_{l_i}^{l_{i+1}} l^3 l^3\,dl} = \frac{\frac{1}{7}\left(l_{i+1}^7 - l_i^7\right) - l_i^6(l_{i+1}-l_i)}{\frac{1}{7}\left(l_{i+1}^7 - l_i^7\right)} = 1 - \frac{r-1}{r^7-1} = 0.549607 \end{aligned}\right\} \tag{36}$$

where

$$r = \frac{l_{i+1}}{l_i} = \frac{\bar{l}_{i+1}}{\bar{l}_i} = 2^{1/3}$$

Equation 26 gives $N_b(t,l) = \int_0^1 6x^2/l^3\,dx = 2$, so Eq. 31 gives

$$\begin{aligned} S_i &= \frac{1}{l_{i+1}-l_i}\int_{l_i}^{l_{i+1}} l^3\,dl \Bigg/ \left(\left(\sum_{j\le i} b_{j,i}\right) - 1\right) \\ &= \frac{1}{l_{i+1}-l_i}\frac{l_{i+1}^4 - l_i^4}{4} \Bigg/ (1.35118 + 0.549607 - 1) \\ &= l_i^3 \frac{r^4-1}{r-1}\frac{1}{4\times 0.9009} = 1.623 l_i^3 \end{aligned} \tag{37}$$

These last results (Eqs. 36 and 37) can now be used directly in Eqs. 23 and 25 to give an explicit set of ODEs.

As Figure 1 shows, the method is capable of predicting the moments of the GSD satisfactorily and the shape of the GSD itself with great accuracy. The most obvious error is that the zeroth moment is slightly overestimated, probably as a consequence of the approximation inherent in Eq. 30. The third moment, however, is correctly predicted as unchanging.

While this example has been chosen with some care to allow the integrations in Eqs. 31 and 34 to be performed analytically, it is possible to perform these tasks numerically for

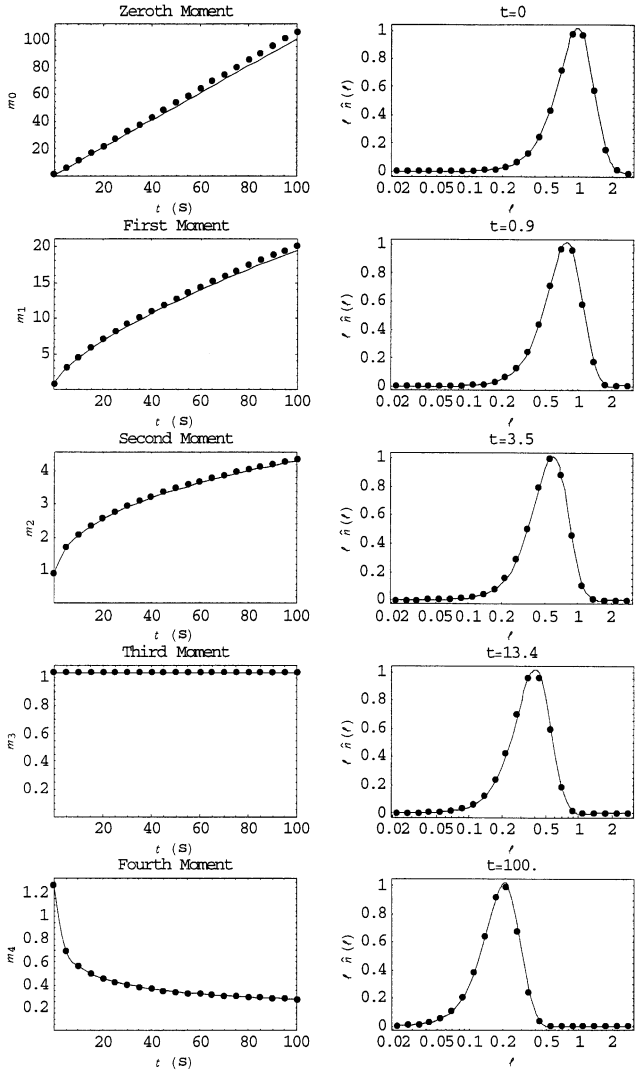

Figure 1. Exact and numerical solutions to PBE for breakage test problem.

The figures on the left show the un-normalized moments n; those on the right show the normalized density function.

any formulation of b or S. An alternative, approximate formulation is to evaluate N_b and V_b numerically as

$$N_{b,i} = \int_0^{\bar{l}_i} b\left(x, \bar{l}_i\right) dx \quad \text{and} \quad V_{b,i} = \int_0^{\bar{l}_i} b\left(x, \bar{l}_i\right) dx \tag{38}$$

and then defining $b^+_{i,j} = 0.443094(l_{i+1} - l_i) b(\bar{l}_i, \bar{l}_i)$ and $b^+_{j,i} = (l_{j+1} - l_j) b(\bar{l}_j, \bar{l}_j)$, calculate

$$b_{j,i} = \frac{V_{b,i} b^+_{i,i}}{\sum\limits_{j \le i} \bar{l}_j^3 b^+_{j,i}} \tag{39}$$

$$S_i = \frac{S\left(\bar{l}_i\right)\left(N_{b,i} - 1\right)}{\sum\limits_{j \le i} b_{j,i} - 1} \tag{40}$$

Discretized Population Balance Equation for the TMD. DPBEs for the tracer-mass distribution are now developed. The process is entirely analogous to that used above so only the result and a brief commentary will be given. The DPBE itself is

$$\frac{dM_i}{dt} = B^A_{1,i}(t) - D^A_{1,i}(t) + B^B_{1,i}(t) - D^B_{1,i}(t) \tag{41}$$

Aggregation. In our original development of Eq. 24, we identified four mechanisms by which granules contribute to the ith interval. Two give rise to new material in the ith interval, two remove material from it. Each of these mechanisms gives rise to $N_i N_j$ terms; in the tracer DPB, these are replaced with $N_i M_j$ terms. The same four mechanisms continue to apply when considering the tracer DPBE, however, those that give rise to formation must allow for both $N_i M_j$ and $M_i N_j$ terms while those that remove material should only include $M_i N_j$ terms. The resulting expression is

$$\begin{aligned} B^A_{1,i}(t) - D^A_{1,i}(t) &= M_{i-1} \sum_{j=1}^{i-2} 2^{j-i+1} \beta_{i-1,j} N_j \\ &+ N_{i-1} \sum_{j=1}^{i-2} 2^{j-i+1} \beta_{i-1,j} M_j + N_i \sum_{j=1}^{i-1} \left(1 - 2^{j-i}\right) \beta_{i,j} M_j \\ &+ \beta_{i-1,i-1} N_{i-1} M_{i-1} - M_i \sum_{j=1}^{i-1} 2^{j-i} \beta_{i,j} N_j - M_i \sum_{j=i}^{n_{\text{eq}}} \beta_{i,j} N_j \end{aligned} \tag{42}$$

As a test of this formulation consider the problem posed by Ilievski and Hounslow (1995). They considered a well-mixed continuous process initially at steady state to which a spike of monodisperse tracer was added. The active mechanisms are size-independent aggregation and nucleation. The analytical forms of the PBEs are

$$\frac{\partial n(t,v)}{\partial t} = \left(\bar{B}^A_0 - \bar{D}^A_0\right) + B^0 \delta(v) - \frac{n(t,v)}{\tau}$$

$$n(t,0^-) = 0, \qquad \left.\frac{\partial n(t,v)}{\partial t}\right|_{t=0} = 0 \tag{43}$$

$$\frac{\partial M(t,v)}{\partial t} = \left(\bar{B}^A_1 - \bar{D}^A_i\right) - \frac{M(t,v)}{\tau}$$

$$M(t,0^-) = 0, \qquad M(0,v) = \delta(v - v_0) \tag{44}$$

Ilievski and Hounslow show that the total mass of tracer decays away exponentially as $e^{-t/\tau}$ and that the tracer-weighted mean particle volume is

$$\bar{v}_T(t) = \frac{\int_0^\infty v M(t,v)\, dv}{\int_0^\infty M(t,v)\, dv} = 1 + \beta_0 B^0 \tau t \tag{45}$$

The DPBEs are

$$\frac{dN_i}{dt} = B^A_{0,i}(t) - D^A_{0,i}(t) + B^0 \delta_{i,0} - \frac{N_i}{\tau}$$

$$\text{which is initialized by setting } \frac{dN_i}{dt} = 0 \tag{46}$$

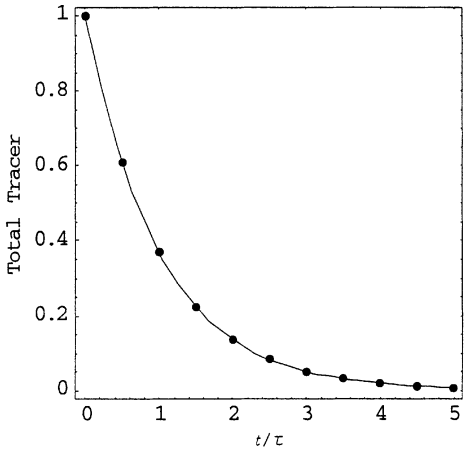

Figure 2. Total mass of tracer in the aggregation test problem.

The markers show the numerical solution from Eq. 47 and the line shows the analytical exponential decay.

$$\text{and } \frac{dM_i}{dt} = B^A_{1,i}(t) - D^A_{1,i}(t) - \frac{M_i}{\tau}$$

$$\text{which is initialized with } M_i(0) = \delta_{i,1} \quad (47)$$

A simulation was conducted with $B^0 = \tau = v_0 = 1$ and $\beta_0 = 4$. Figure 2 shows that the calculated total tracer mass does indeed decay away exponentially. Similarly, Figure 3 shows that the numerical and analytical tracer-weighted mean particle volumes are in very close agreement. We conclude that the DPBE described by Eq. 42 is a good representation of the underlying PBE.

Breakage. The breakage form of the tracer DPBE is a very simple modification of Eq. 25.

$$B^A_{1,i} - D^A_{1,i} = -S_i M_i + \sum_{j=i}^{n_{eq}} 2^{i-j} b_{i,j} S_j M_j \quad (48)$$

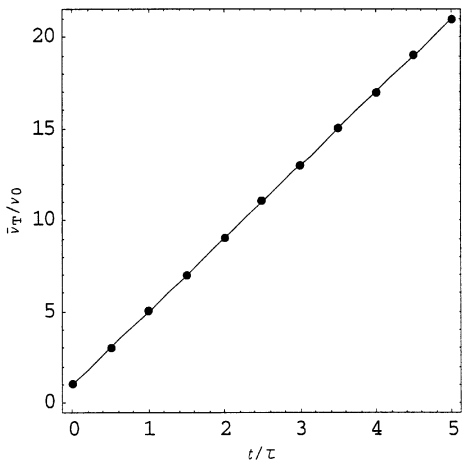

Figure 3. Tracer-weighted mean particle volume for aggregation test problem.

The markers show the numerical solution from Eq. 47; the line shows the analytical solution from Eq. 45.

The modification comes about by comparing Eqs. 18 and 19 with Eqs. 13 and 14: a factor equivalent to the v/ϵ in Eq. 18 is required. The term 2^{i-j} is that factor. Equation 48 was checked by first determining that it yields constant tracer mass in batch systems and then, that in cases when tracer is initially uniformly distributed, the TMD remains identical.

Extracting rate constants

We use two methods for extracting the rate constants from our data. The first, a *differential* method, removes the need to assume a form for the time dependence of the rate constants, but is susceptible to noise in the experimental data. The second method uses an integral technique which does require an assumed form of the time dependence.

Differential Technique. Bramley et al. (1996) present a method for extracting the time dependence of the various rate constants from measurements of the size distributions. They considered nucleation, growth, and aggregation, basing their calculations on the zeroth and third moments of particle-size distributions; we show here how the method may be extended to include breakage and other mechanisms while being generalized to arbitrary moments.

The essence of the method is to exploit the linearity in the relationship between the rate of change of granule numbers and the various kinetic parameters. A DPBE may be written as

$$\begin{bmatrix} \frac{dN_1}{dt} \\ \frac{dN_2}{dt} \\ \vdots \end{bmatrix} = \frac{d\boldsymbol{N}}{dt} = \begin{bmatrix} \phi_{1,1}(\boldsymbol{N})p_1 + \phi_{1,2}(\boldsymbol{N})p_2 + \cdots \\ \phi_{2,1}(\boldsymbol{N})p_1 + \phi_{2,2}(\boldsymbol{N})p_2 + \cdots \\ \vdots \end{bmatrix} = \boldsymbol{\phi}(\boldsymbol{N})\boldsymbol{p} \quad (49)$$

where $\boldsymbol{N}$ is the vector of (measured) N_is, $\boldsymbol{p}$ is a vector of parameters and $\boldsymbol{\phi}$ is a matrix of coefficients that depend only on the (known) values of the N_i. The $\boldsymbol{p}$ are the *size-independent* portions of the rate constants such as if the aggregation rate constant is written as $\beta(t, l_1, l_2) = \beta_0(t) \times \beta_1(t, l_1, l_2) \times \beta_2(l_1, l_2)$ where β_1 and β_2 are known functions. Then the parameter to be determined is $\beta_0(t)$. Similarly, the size-independent portions of the selection rate constant $S_0(t)$, the growth rate $G_0(t)$, the nucleation rate constant $B^0_0(t)$, and the sink function $O_0(t)$ may be added. In its maximum extent, then $\boldsymbol{p} = (B^0_0(t),\ G_0(t),\ \beta_0(t),\ S_0(t),\ O_0(t))$. The key point is that the relationship between the rate of change of numbers in an interval and the parameters is linear, and the coefficients in that linear relationship, $\phi_{1,1}$, $\phi_{1,2}$, and so on, may be calculated from the known, experimental values of the N_is. It follows, then, that any linear combination of the rates of change will also depend on the parameters in a linear fashion. For example, the rate of change of the jth moment is given by

$$\frac{dm_j}{dt} = \sum_i \tilde{l}^j_i \frac{dN_i}{dt} = \tilde{\boldsymbol{l}}^j \cdot \frac{d\boldsymbol{N}}{dt} = \tilde{\boldsymbol{l}}^j \cdot [\,\phi_1(\boldsymbol{N})p_1, \phi_2(\boldsymbol{N})p_2 + \cdots\,]$$

$$= \tilde{\boldsymbol{l}}^j \cdot [\,\boldsymbol{\phi}(\boldsymbol{N})\boldsymbol{p}\,] \quad (50)$$

where $\bar{\boldsymbol{l}}^j = (\bar{l}_1^j, \bar{l}_2^j, \cdots)$ is the vector of average sizes of each interval raised to the power j. Equation 50 provides a linear relationship between the unknown $\boldsymbol{p}$ and the experimentally determinable rates of change of the moments. The method requires simply that the same number of equations as there are unknown parameters to be created by Eq. 50; these may then be solved for the values of the $\boldsymbol{p}$. For example, in the next section simultaneous aggregation and breakage will be considered. $\boldsymbol{p} = (\beta_0(t), S_0(t))$, so two equations are required. These are generated from Eq. 50 by setting $j = 0$ and $j = 4$ to give

$$\frac{dm_0}{dt} = \bar{\boldsymbol{l}}^0 \cdot [\boldsymbol{\phi}(\boldsymbol{N})\boldsymbol{p}]$$

$$\frac{dm_4}{dt} = \bar{\boldsymbol{l}}^4 \cdot [\boldsymbol{\phi}(\boldsymbol{N})\boldsymbol{p}]$$

At every time-point dm_0/dt and dm_4/dt can be estimated, and $\phi(\boldsymbol{N})$ calculated from Eqs. 24 and 25. Thus, at every time-point, $\boldsymbol{p} = [(\beta_0(t), S_0(t)]$ may be determined.

The choice of equations to use depends to a certain extent on the method for collecting the data and on the active processes. If a mass-sensitive device is used, m_3 and m_4 are good choices, if a number sensitive device, m_0 and m_1 work well. If aggregation is active, m_0 is an obvious choice since aggregation affects that moment strongly, while m_3 would be a poor choice, since it does not depend on the aggregation rate. Similarly, growth suggests m_1 or m_3 but not m_0. When considering nucleation, a single row (the first one) of Eq. 49 is a good choice, since the rate of change of numbers in the first interval is strongly dependent on the nucleation rate.

The authors' experience is that with good quality data, two or three parameters may be estimated quite reliably in this way. However, the presence of moderate noise or a higher-dimensioned parameter space, which results in ill-conditioned equations, yields results of limited value. In this case the following integral technique is more appropriate.

Integral Technique. As an alternative to the differential technique, we can pose the rate extraction problem as a simple chi-square minimization process in the manner of Press et al. (1992). The parameters to be estimated now are not the rate constants themselves, but some set that relates the rate constants to time (or some variable that depends on time or time and the vector $\boldsymbol{N}$), for example, the p_i in

$$\beta_0(t) = p_0 + p_1 t$$
$$S_0(t) = p_2 e^{-p_3 t} \tag{51}$$

Define the predicted size distributions as a set of $\tilde{N}_i(t_k, \boldsymbol{p})$ and the observed distribution as the set of $N_i(t_k)$, then chi-square is

$$\chi^2(\boldsymbol{p}) = \sum_i \sum_k \left\{ \frac{\left[N_i(t_k) - \tilde{N}_i(t_k, \boldsymbol{p}) \right]^2}{\sigma_{i,k}^2} \right\} \tag{52}$$

The selection of $\boldsymbol{p}$ becomes $\min_{\boldsymbol{p}} \chi^2(\boldsymbol{p})$. This formulation of the problem is most useful when the individual N_i are uncorrelated, and the variances $\sigma_{i,k}^2$ are known. Neither of those situations applies here: the best estimate of the variance is that the error in each value of N_i scales as $\bar{l}_i^{-3}$ giving constant relative error in *mass* in each interval.

Modeling environment

All the numerical methods described here were implemented as a *Mathematica* package *DPB*, details of which can be found on the Web (Hounslow, 1999).

Results

Our intention here is to show that the developed PBEs are capable of describing our experimental results in some considerable detail. We will show that it is possible to choose a set of kinetics that appear to describe the size distribution well, but when used in predictions of the tracer distribution, are quite unsatisfactory. It must be emphasized, however, that we are not seeking to identify the "true" kinetics for our system. The reason for this limitation in our ambition is identified in our recent work (Scott et al., 2000), where we show that the properties of granules vary quite considerably with size. For example, the binder is frequently quite maldistributed across the size range and the nature and extent of that maldistribution change with time. It is likely that the "true" kinetics for interactions between pairs of granules and the breakage of individual granules depend quite strongly on the binder content of the granules concerned. For this reason, binder content ought to be added to the list of internal coordinates and the kinetics ought to relate the rate constants to size and binder content. In the context of our current work we must take a mean-field approach to this matter, allowing that the distribution of binder with size can be characterized by a size dependence term and that the changing maldistribution may be described by a time dependence of the rate constants. Neither of these is a true fundamental description, so "true" kinetics are beyond our scope.

Initial models

Part of our motivation for conducting tracer experiments was as a means of identifying the breakage function. For example, in Figure 4 we show the tracer distribution one minute after the addition of a spike of tracer in the size range 1,000 to 1,180 μm. There is a clear mode of material at 160 μm. We interpret this as being the distribution of fragment sizes and, thus, indirectly, as the breakage function. The line drawn through the mode is a scaled log-normal distribution with a mass geometric mean size $\bar{l}_{gv} = 160$ and geometric standard deviation $\sigma_g = 1.70$. An appropriate formulation of the fragment distribution is

$$b_f(x,l) = \left(\frac{l}{x}\right)^3 \frac{\dfrac{1}{x\sqrt{\pi/2}\,\ln\sigma_g} \exp\left[-\left(\dfrac{\ln x/\bar{l}_{gv}}{\sqrt{2}\,\ln\sigma_g} \right)^2 \right]}{1 + \operatorname{erf}\left[\dfrac{\ln l/\bar{l}_{gv}}{\sqrt{2}\,\ln\sigma_g} \right]} \tag{53}$$

The numerator in this expression is the standard log-normal-probability density function, the denominator is the cumulative form of the log-normal distribution present here to normalize the log-normal term since it is defined on $x \in (0, \infty)$ whereas the breakage function is defined on $x \in (0, l)$. Fi-

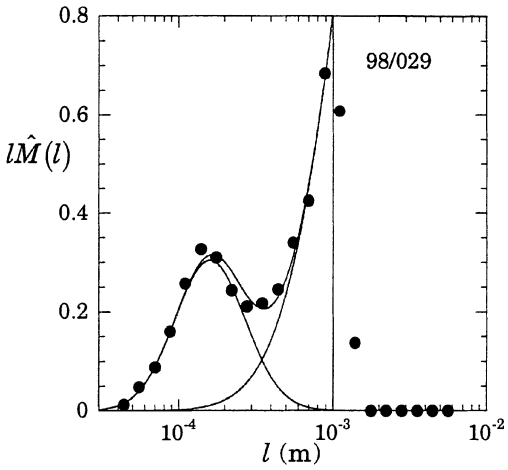

Figure 4. Normalized tracer distribution 1 min after adding tracer in the size range 1,000 to 1,180 μm.

The initial model for breakage interprets the distinct small-size mode as the size-distribution of breakage fragments; the refined model treats all the material smaller than 1,000 μm as fragments. The curves drawn are truncated log-normal distributions with $\bar{l}_{g_v} = 160$ μm and $\sigma_g = 1.70$ (mode 1), and $\bar{l}_{g_v} = 3.8$ mm and $\sigma_g = 2.66$ (mode 2), corresponding to Eq. 53 with $l = 1$ mm. The remaining line is the sum of the other two.

nally, the leading term $(x/l)^3$ converts the mass distribution of Figure 4 into the number distribution required and ensures the conservation of mass.

Pearson et al. (2001) show that the selection rate-constant is size independent, and that it has an initial value of approximately 0.01 s^{-1}. We found that simulations taking this value grossly overestimate the breakage rate and that a value of 0.001 s^{-1} is more appropriate. Why this might be so, is addressed in the next section.

Many forms of the aggregation kernel have been proposed. Here we investigate the use of three (see Table 1): the size-independent kernel (SIK), Smoluchowski's (1917) shear kernel (SSK), and the equipartition of kinetic energy kernel (EKK). We choose the first of these on the grounds of simplicity and a desire not to add complexity to models when the accuracy of the data do not warrant it; the other two kernels are chosen as they both have a sound physical basis. SSK assumes that granules collide as a consequence of a shearing motion (which is certainly to be encountered in a high-shear mixer), while the EKK assumes that collisions occur as a consequence of random motion—that random motion being apportioned to partition kinetic energy uniformly among all sizes of granules (in the manner of an ideal gas). We have taken the approach of using kernels that reflect some physical mechanism for the collision process as it is our intention eventually to represent the aggregation rate as the product of collision rates and aggregation efficiency (the fraction of collisions that result in aggregation events). Just such an approach has recently yielded considerable insight into an analogous process during crystallization (Hounslow et al., 2001). These kernels also give a broad range of the types of size dependence that might be encountered. The SIK, of course, favor all interactions equally (in proportion to the population of granules of each size), but SSK and the EKK favor quite distinct and different kinds of interactions. SSK favors interactions involving large granules and, therefore, large-large interactions dominate. The EKK on the other hand favors large granules as they sweep out more area and small ones as these granules are more mobile, as a consequence large-small interactions are favored.

Figure 5 shows some results of the initial simulations using the three different kernels. The values for the time-dependent portion of the kernels were deduced using the differential method of Eq. 50 (with $j = 4$). It is no surprise that the 4,3 mean size is well-predicted by all three kernels, since the results have been fitted to the rate of change of the fourth moment. The GSD predictions, however, allow discrimination between the three: SSK is quite incapable of describing the evolving GSD—it fails to move the small-sized mode and translates the large-size mode too far. The other two kernels both represent the final GSD quite well, although they fail to predict the shoulder at small sizes. In Figure 6 it can be seen that SSK places the tracer in the wrong positions, and that the SIK and the EKK both deal well with the vestigial spike at 1,100 μm, but both fail to predict the merging together of the two modes in the TMD. None of the models used show the correct initial decline in the tracer-weighted mean size.

Table 2 shows these results in quantitative form with results summed over all times (by contrast to Figure 5 and Figure 6 which show results only at the end of an experiment). The goodness-of-fit to the GSD shows that the EKK is substantially superior to the other two kernels. The goodness-of-fit to the TMD shows, surprisingly, that SSK gives the best description of the tracer data. However, none of the models presented so far are particularly successful in that respect, that SSK is slightly superior seems to arise from a general smearing out of results, whereas the EKK overpredicts the height of the small-size mode.

It is concluded from these initial simulations that SSK is not capable of describing the GSD and the EKK gives the

Table 1. Aggregation Kernels Considered

Name	Form $\beta(l,\lambda)$	Size Dependence: Like Interactions $l \approx \lambda$	Size Dependence: Unlike Interactions $\beta(L,l)$, $L \gg l$	Comment
Size-independent kernel SIK	$\beta_0(t)$	1	1	All events equally probable
Smoluchowski's shear kernel SSK	$\beta_0(t)(l+\lambda)^3$	l^3	L^3	Large-large events favored
Equipartition of kinetic energy kernel EKK	$\beta_0(t)(l+\lambda)^2\sqrt{\frac{1}{\lambda^3}+\frac{1}{l^3}}$	$l^{1/2}$	$L^2/l^{3/2}$	Large-small events favored

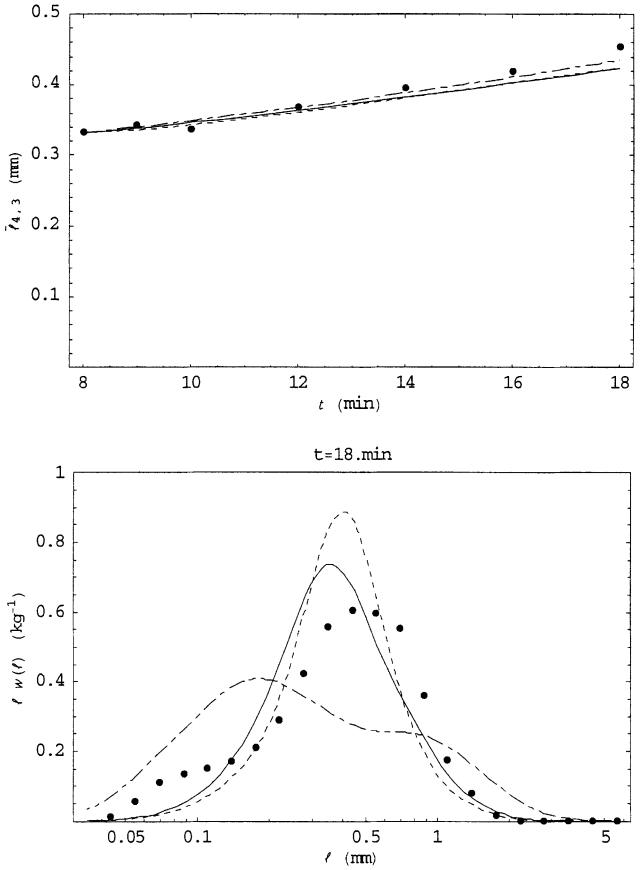

Figure 5. Granule-size distribution results of initial simulations using SIK (dotted line), SSK (chain-dashed line) and EKK (continuous line).

(a) The 4,3 mean-size as a function of time; (b) the mass-weighted GSD at the end of an experiment.

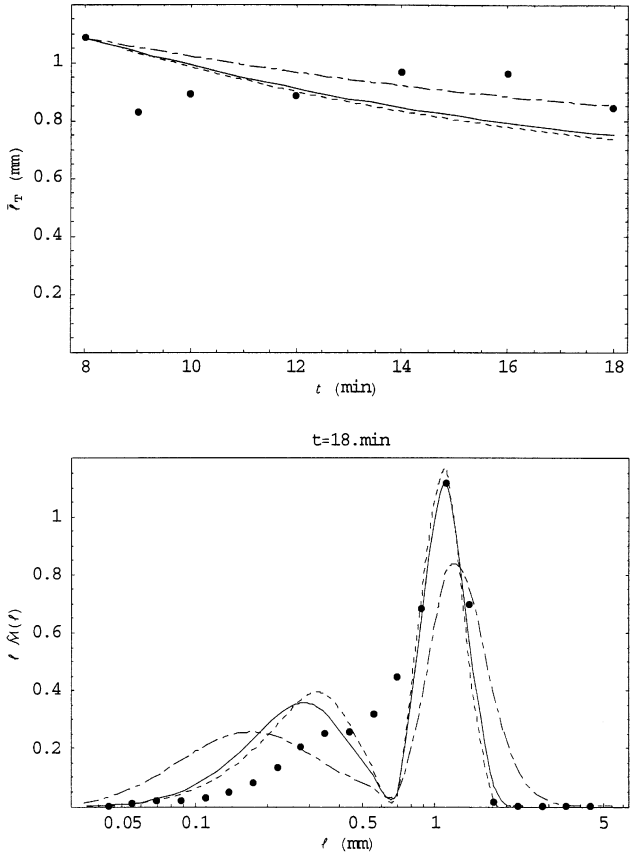

Figure 6. Tracer-mass distribution results of initial simulations using SIK (dotted line), SSK (chain-dashed line) and EKK (continuous line).

(a) The tracer-weighted mean-size as a function of time; (b) normalized TMD at the end of an experiment.

best description. It is further concluded that the breakage and selection models require refinement.

Refined model

In all of the tracer-mass distributions considered in the previous section the models failed to predict the smooth blending of the small-size mode (attributed to the fragment of the original tracer granules) and the large-size mode (stemming from the original spike of tracer granules). Furthermore, plots of the tracer-weighted mean size (such as Figure 6a) all show an immediate decrease followed by a gradual rise.

Bimodal Breakage Model. In developing the model used for breakage in the previous section it was assumed that whenever a granule is selected for breakage, it is broken entirely into small fragments; no large pieces remain. We believe that the blending of the two modes referred to above arises as a consequence of the generation of relatively large fragments of material in addition to the small fragments.

Figure 7 shows how we propose breakage proceeds. When a granule breaks, it produces two kinds of fragments: many fine ones of mass-mean size near 150 μm, and a few large ones of mass-mean size, somewhat less than that of the initial granule. In this way the breakage curve is, on a mass basis, bi-modal. The bi-modal distribution shown in Figure 4 is de-

Table 2. Goodness of Fit for Initial Simulations

	Goodness of Fit	
	GSD	TMD
Kernel	$\chi^2(\boldsymbol{p}) = \sum_i \sum_k \left[(\hat{W}_i(t_k) - \tilde{\hat{W}}_i(t_k, \boldsymbol{p}))^2 \right]$	$\chi^2(\boldsymbol{p}) = \sum_i \sum_k \left[(\hat{M}_i(t_k) - \tilde{\hat{M}}_i(t_k, \boldsymbol{p}))^2 \right]$
SIK	0.070	0.38
SSK	0.081	0.28
EKK	0.037	0.32

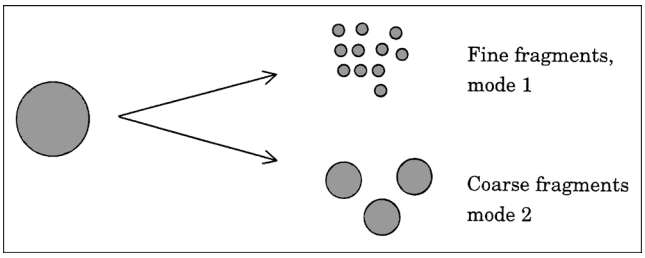

Figure 7. Bimodal breakage model.

duced from a breakage function comprising the sum of two truncated log-normal distributions

$$b(x,l) = 0.484 b_{f,1}(x,l) + 0.516 b_{f,2}(x,l) \qquad (54)$$

where $b_{f,1}$ and $b_{f,2}$ are of the form given in Eq. 53 with $\bar{l}_{gv} =$ 160 μm, $\sigma_g = 1.70$ (mode 1), and $\bar{l}_{gv} = 3.8$ mm, $\sigma_g = 2.66$ (mode 2), respectively. These parameters are a least-squares fit to the data shown.

It follows from this that when a 1 mm granule breaks, it forms, on average, 7.5 large fragments and 420 small fragments, with nearly equal masses of each being generated.

Selection. Plots of the tracer-weighted mean-size suggest that the initial breakage rate is considerably greater immediately after the tracer granules are added, rather than at later times. Figure 7 in Pearson et al. (2001) tends also to support this hypothesis, since the rate of relegation of the tracer is considerably greater for the younger granules than it is for those of greater ages, a point made quantitatively in the previous section where we found that the observed initial selection rate constant of 0.01 s^{-1} is an order of magnitude higher than the apparent average rate over an experiment. We now propose that breakage effectively ceases after the first minute or so beyond the addition of the tracer, that is, by $t = 10$ min. We propose that this should be described by an exponential decay in selection rate constant with a time constant of 20 s. The expression used has one parameter S_A

$$S(t,l) = S_A \exp\left(-\frac{t-480}{20}\right) \qquad (55)$$

Aggregation Model. The simplicity and success of the EKK in describing our results in the early stages of our work lead us to adopt it for the more detailed analysis. Iterative application of both the integral and differential methods described earlier identified that the value of β_0 changed little with time and any variation that was observed might be accounted for by a simple linear dependence on time.

$$\beta_0(t) = \beta_A + \beta_B(t-480) \qquad (56)$$

Parameters to be Estimated. Next, three parameters will be estimated, S_A, β_A, and β_B by means of the integral fitting technique. However, it must be acknowledged that a number of parameters have already been formally fitted to the data; the six parameters of Eq. 54 were obtained by fitting to the data of Figure 4 and the time constant of 20 s in Eq. 55 was selected as reflecting the rate of decline in breakage, shown in Part I (Pearson et al., 2001) of this pair of articles, and so is in some sense also fitted. It would in principle be possible to use the fitting technique to select all these parameter values, and, therefore, perform a search in a 10-D parameter space. In fact, such a search would be prohibitively expensive in computing resource and unlikely to converge. The approach adopted here of using a single time point (that is, Figure 4) to fit the parameters of Eq. 54 and engineering insight to estimate the time constant of 20 s reduces the problem to a tractable size, while focusing on the results of greatest interest: the rate constants. It follows that the values for these rate constants calculated below, and, in particular, their errors, reflect the choices made for these other parameters and are not in that sense the global optimal set.

Fitting the Model. Fitting the model to the data requires the selection of three parameters $\boldsymbol{p} = (S_A, \beta_A, \beta_B)$. This was achieved using an integral technique with χ^2 given by

$$\chi^2(\boldsymbol{p}) = \sum_i \sum_k \left\{ \left[\hat{W}_i(t_k) - \hat{\tilde{W}}_i(t_k, \boldsymbol{p}) \right]^2 \right\} + \sum_k \sum_i \left[\hat{M}_i(t_k) - \hat{\tilde{M}}_i(t_k, \boldsymbol{p}) \right]^2 \qquad (57)$$

In this way the errors in the normalized values of the tracer distribution are implicitly assumed to be of the same order as those in the normalized granule mass distribution. Three different tracer sizes were considered, with, in each case, six time intervals to be simulated and 22 size intervals. This was achieved by the simultaneous solution of the DPBEs (Eqs. 41 and 23) with the EKK (Table 1), the bi-modal breakage function (Eq. 54), and with the exponentially decaying selection function, Eq. 55, to predict the 792 experimental data points.

The fitting exercise yielded $\beta_A = 1.30\ (\pm 0.070) \times 10^{-9}$ kg·$m^{1/2}$ s^{-1}, $\beta_B = -6.\ (\pm 3.) \times 10^{-13}$ kg·$m^{-1/2}$·s^{-2}, and $S_A =$ 0.025 ($\pm$0.001) s^{-1}. Where the errors shown are $\pm$ one standard error. It may be concluded that the dependence on time of the aggregation rate constant is only just statistically significant, but that the time-independent portion is very well defined, as is the selection rate.

Simulation results

Results are now presented for experiments with tracers of three different sizes: large tracer granules were added in the size range 1,000–1,180 μm, hereafter referred to as 1,090 μm; medium-sized granules added in the range 500–600, hereafter 550 μm, and small granules added at 180–212 μm, hereafter 206 μm. It is important to note in what follows that all three sets of results, that is, for large, medium and small tracer granules, are described by the same set of kinetics, given in the previous section, that is

$$S(t,l) = 0.025 \exp\left(-\frac{t-480}{20}\right) \qquad (58)$$

$$\beta_0(t) = 1.30 \times 10^{-9} - 6 \times 10^{-13}(t-480) \qquad (59)$$

and the breakage function given by Eq. 54.

Large Tracer Granules. Figure 8 shows the measured and simulated GSDs. The model predicts most of the observed behavior: the mean-size rise slowly at first and then at a reasonably constant rate—probably as a consequence of the ab-

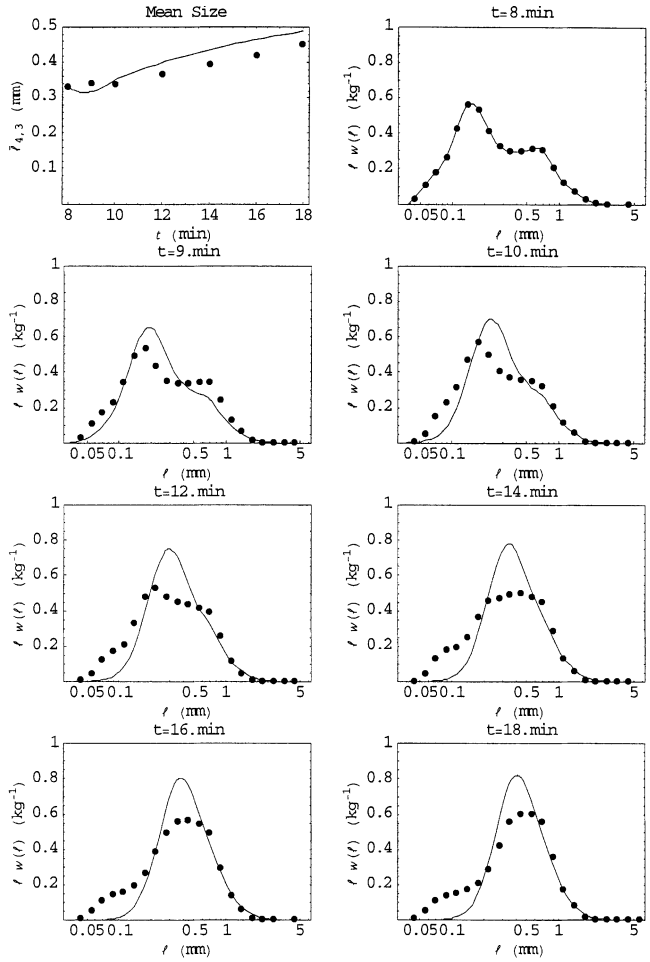

Figure 8. Simulated and experimental granule-size distributions for large (1,100 μm) tracer experiment using kinetics of Eqs. 58 and 59.

The first figure shows the 4,3 mean-size as a function of time. The remaining figures show the mass GSD as it evolves over time.

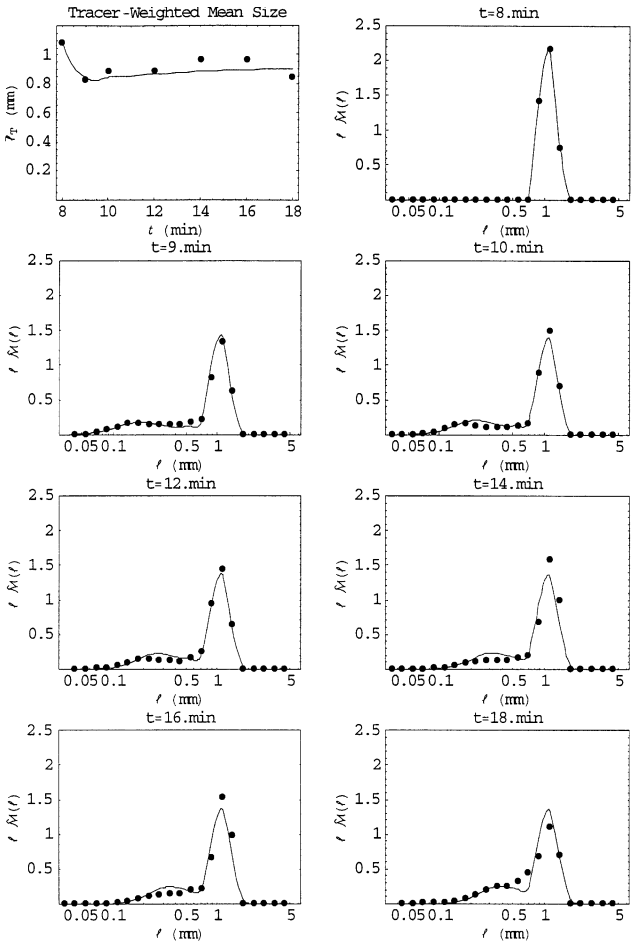

Figure 9. Simulated and experimental tracer-mass-distributions for large (1,100 μm) tracer experiment using kinetics of Eqs. 58 and 59.

The first figure shows the tracer-weighted mean size; the remaining figures show the TMD as it evolves over time.

sence of breakage after $t = 10$ min. The relatively unchanging nature of the aggregation rate constant and the dominant l^2 term in the aggregation size dependence (if capture of material goes as l^2, the rate of increase of diameter of a granule is constant) are an important factor in selecting the EKK. The size distributions themselves match very well at early times, but tend to diverge a little towards the end of the experiment. The cause of the divergence is the small-size shoulder that appears at about $t = 12$ min in the experiments, but not in the simulations. On the basis of GSD data only, it would appear that some modification to the breakage function is required: fragments seem to be created in the sub-100 μm region. However, as will be seen, the TMDs show no sign of such a process.

Figure 9 shows measured and simulated TMDs: the quality of agreement is exceptional. The simulated and experimental tracer-weighted mean-sizes agree within the scatter of the data; the decay in the initial spike of tracer is captured completely (confirming the extent of net breakage); the position and evolution of the fragment distribution are both exceptionally well described. The only defect in the simulations is the mismatch at $t = 18$ min at about $l = 0$ m. If the experimental data are to be believed, the tracer distribution undergoes an abrupt change in this last time interval that is not captured by the model.

Medium-Sized Tracer Granules. Figure 10 shows simulated and measured tracer data for the 550 μm tracer granules. The GSD data are not shown as they are virtually indistinguishable from the control results (Figure 8). The simulations again give a good description of the experimental data. The most obvious deviation is the inability of the simulations to capture the precise shape of the primary tracer peak. This arises, at least in part, for the difficulties inherent in describing sharp peaks with a discretized representation; particularly as the data are collected on a $\sqrt[4]{2}$ progression in size and the modeling is conducted on a $\sqrt[3]{2}$ progression. It is interesting to note that the merging of the two modes is successfully predicted by the model for this experiment.

Small Tracer Granules. Figure 11 shows simulated and measured results for the smallest tracers used, 206 μm. The evolution of the TMD is extremely well described by the model. The location of the mode and the breadth of the dis-

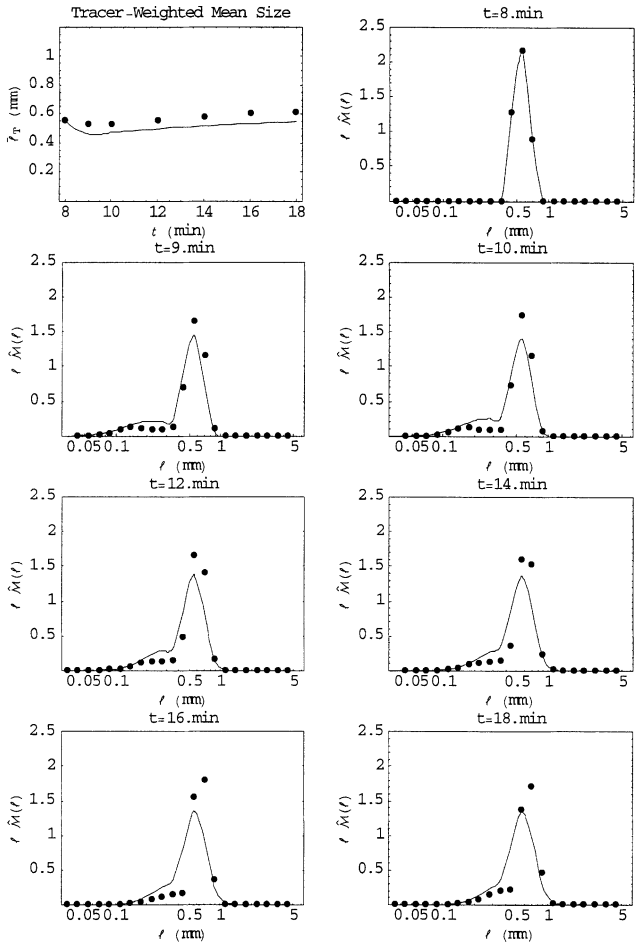

Figure 10. Simulated and experimental tracer-mass distributions for medium-sized (550 μm) tracer experiment using kinetics of Eqs. 58 and 59.

The first figure shows the tracer-weighted mean size; the remaining figures show the TMD as it evolves over time.

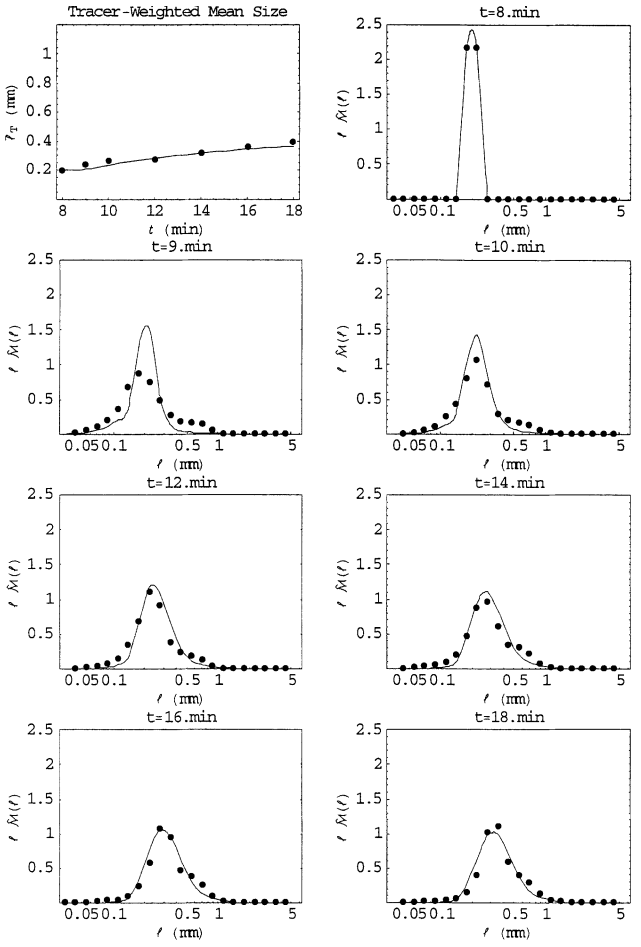

Figure 11. Simulated and experimental tracer-mass distributions for small (206 μm) tracer experiment using kinetics of Eqs. 58 and 59.

The first figure shows the tracer-weighted mean-size; the remaining figures show the TMD as it evolves over time.

tribution are very well predicted for all but $t = 9$ min. The discrepancy visible at that time indicates that the initial selection and aggregation rate constants have perhaps been underestimated.

Discussion

Selection rates

The breakage selection function has been found to decrease rapidly with time. Two sources of evidence may be adduced to support this result. First, the mean-size of granules invariably decreases during the early periods of a granulation experiment. This implies that during this period the net rate of breakage exceeds the net rate of aggregation, which might be as a consequence of a decline in the former or of an increase in the latter. However, the second source of data, the tracer-mass distributions, provides strong evidence that it is the decline in breakage rates that is the cause. Distributions, such as those shown in Figure 9 to Figure 11, all show a dramatic initial decline in the magnitude of the tracer peak followed by an extended period of very little change. This can only arise from significant breakage initially followed by a period of negligible breakage. This point is further accentuated by the initial decline in the tracer-weighted mean-size followed by its subsequent gradual increase.

The changing selection rate of granules must be as a consequence of the changing properties of those granules. We now put forward two hypotheses to account for this change. The first is that granules in a particular size-class gradually become stronger with time—we term this the homogeneous strength increase hypothesis—probably as a consequence of granule compression and other liquid-to-solid ratio changing mechanisms. Figure 3 in Pearson et al. (2001) shows that, between 8 and 12 min, the average liquid-to-solid ratio for the 1,100 and 550 μm tracer granules is decreasing while the 196 μm granules is, perhaps, increasing. It might well be that the large granules are too wet and the smallest too dry, for optimum strength. The alternative hypothesis that we term is the heterogeneous strength hypothesis: within any size-class, there exists a distribution of strengths. When tracer granules are added, the weaker granules rapidly break leaving only a strong, nonbreaking residue. In this case the firt-order decay of the selection function Eq. 55 would be entirely appropriate. The most likely explanation for a distribution of strengths

within any one-size-class is nonuniformity, that is, heterogeneity, in liquid-to-solid ratios.

While we have absolutely no conclusive evidence to demonstrate that either hypothesis holds, the information we do have on average liquid-to-solid ratios within a size-class makes it seem unlikely that much variation in selection rates would be observed. We propose, tentatively, that the heterogeneous strength hypothesis holds.

Further evidence of heterogeneity within a size-class might also be inferred from the stationary small-size shoulder visible in Figure 8, and discussed above. A plausible explanation for this result is that a population of small, dry fragments is generated by breakage events, possibly at nucleation, and that these granules, unlike their wetter colleagues within their own size-class, are unable to aggregate with other granules.

Breakage function

In our refined model we found it necessary to describe the breakage function with a bimodal distribution. We found that our initial assumption that only fine fragments are formed from each breakage event was not capable of predicting the fine detail of the tracer-mass distributions. The refined model allowed that two types of fragments are formed: large ones which number fewer than ten per breakage event, and small ones that number in the hundreds. Direct experiment observation of breakage rates is needed to confirm this result.

Aggregation rate constant

The literature is replete with curve fitting exercises used to identify aggregation kernels for granulation processes. Unfortunately, the ill-conditioned nature of the inverse problem (Muralidar and Ramkrishna, 1986) means that a kernel giving a good description of a set of data is far from unique. How then does the current study differ from these exercises in curve fitting? In part it does not: the model selected, the EKK, was chosen because the curves deduced fitted the measured granule-size distributions. However, we argue that our choice is far more than just curve fitting. Most importantly, this kernel is capable of describing both the granule-size distribution and the tracer-mass distribution. It is significant that it is able to do so when tracer was added in quite narrow bands. Inspection of Figures 9 to 11 shows that the EKK is capable of describing the motion of the small-size mode and the original peak along the size axis for all three sizes of tracer. The last figure in particular is important as it shows that the model is capable of predicting the shape of the tracer distribution after the two modes have combined and the original peak has vanished. The shape of this distribution is determined largely by the form of the kernel.

It is also reassuring that the kernel is only weakly time-dependent. The gradual decline, in its value, that our fitting suggests, might be attributable to the gradual equalization of liquid-to-solid ratio across the size spectrum, or, on the other hand, might not be significant. Had we chosen a kernel that was strongly time-dependent, a much more convincing explanation would be required.

We cannot conclude that the success of the EKK arises because collisions in a high shear mixer occur at the frequency it implies—after all, some account of the size dependence for the efficiency with which a collision gives an aggregate needs to be considered. We can, however, propose that small-large events are preferred, that a large granule gathers small ones at a rate proportional to the projected area of the large granule, and perhaps inversely proportional to the size of the small ones to the power 1.5. Verification of this point is likely to require direct video observation of the motion and collision of aggregates.

Conclusions

The key points to be taken from this work are

• A new discretized population balance equation (DPBE) for breakage (Eqs. 25, 31 and 34) has been developed. As Figure 1 shows, the method is capable of high quality results. Unlike other DPBEs developed by our group, this result for breakage requires the evaluation of a number of constants for each formulation of the breakage and selection function used. These constants are in fact integrals, and although they need only be determined once for any given formulation, the computational burden, should they need to be determined numerically, is significant. Therefore, it is particularly convenient to implement the method in a system that supports symbolic manipulation, allowing the integrals to be determined analytically, but by computer. Our implementation is the *Mathematica* package *DPB*.

• A population balance equation (PBE) (Eq. 15 with Eqs. 16 to 19) and an associated DPBE for *tracers* (Eq. 41 with Eqs. 42 and 48) have been developed. The DPBE has been shown in Figure 2 and Figure 3 to yield results entirely in agreement with the PBE.

It is important to note that the formulation of both forms of the PBE requires the assumption that none of the rates of a process depend on any variable other than time and granule size. In particular, the rates must not depend on the tracer content of any one granule. For an inert material, such as a tracer, this is no great restriction, but it does migitate against the use of these equations to represent, say, the distribution of binder liquid (so the second internal co-ordinate would be mass of binder, rather than mass of tracer) since we do expect the rates to be a function of the binder contained within individual granules.

It is further assumed within both forms of the PBE that, when a tracer-containing granule breaks, all the resulting fragments contain equal concentrations of tracer.

• A generalized differential method for extracting rate constants from PBEs (Eq. 49) has been developed. Primarily its use here is as a method for developing initial guesses to be used within the integral technique, also described here.

• The selection rate constant in our experiments has been shown to decline rapidly with time, perhaps exponentially with a time constant of 20. We tentatively put forward a heterogeneous strength hypothesis to explain why this should be so. We have also proposed that some small granules fail to grow because of heterogeneity in liquid distribution within size-classes. Direct experimental data are needed to test this hypothesis.

• We have interpreted our tracer data to conclude that breakage events give rise to two groups of fragments: large granules near-in-size to the parent granule and small granules approximately 100 μm in size. Consequently, on a mass basis, the breakage function is bi-modal. Direct experimental

observation of breakage events is required to test this hypothesis.

• We have adapted the collision rate model from the kinetic theory of ideal gases to model the rate of aggregation events between granules in a high-shear mixer. This collision rate constant, termed the EKK, favors large-small interactions and requires the estimation of a size-independent portion $\beta_0(t)$. We find that β_0 depends on time at only the very limits of statistical significance. Direct observation of granule motion is required to verify the mechanistic nature of this result.

• The model derived from this work is capable of describing the granule-size distributions and the tracer-mass distributions simultaneously with great accuracy. For this purpose, three parameters (two if we neglect the dependence on time of $\beta_0(t)$) have been adjusted to fit the model to the data. The same model, with the same parameter values, is able to describe experiments with spikes of tracer ranging in size from 206 to 1,090 μm.

• We have been at pains to point out that time is an unsatisfactory correlating variable for modeling any rate process. The fact that any rate constant seems to depend on time is evidence that some physical property of the system is also varying with time. Real rate-based understanding and "true" kinetics can only be found when that physical property is identified and used as an appropriate driving force perhaps as a property of a size-class, accounting for heterogeneity between size-classes, but more powerfully as a property of individual granules, accounting for heterogeneity within size classes.

Acknowledgment

This work was supported by a CASE award (for J. M. K. Pearson) from the EPSRC of the U.K., by Unilever Research and by Romaco U.K. Ltd.

Notation

b = breakage function, m^{-1} or m^{-3}
B^0 = nucleation rate, $kg^{-1} \cdot s^{-1}$
B = birth term in the 2-D PBE, $kg^{-3} \cdot s^{-1}$
c = mass of tracer in a granule, kg
D = death term in the 2-D PBE, $kg^{-3} \cdot s^{-1}$
f = 2-D population density function, kg^{-3}
G = growth rate, $kg \cdot s^{-1}$
k_v = volumetric shape factor, taken as $\pi/6$
l = granule size, m
m_j = moment, $m^j\ kg^{-1}$ or kg^{j-1}
M = tracer mass density function, m^{-1}
= mass of tracer
N = number of granules, kg^{-1}
n = number density function, $kg^{-1} \cdot m^{-1}$
n_{eq} = number of size intervals
O = sink selection rate constant, s^{-1}
p = a parameter
$\boldsymbol{p}$ = vector of parameters
R = rate, $kg^{-1} \cdot s^{-1}$
S = breakage selection rate constant, s^{-1}
r = ratio of sizes in two adjacent classes
t = time, s
v = particle or granules mass or volume, kg or m^3
w = mass density function, m^{-1}
W = mass of granules, kg

Greek letters

β = aggregation rate constant or kernel, $kg \cdot s^{-1}$
γ = mass of tracer, kg
$\delta(l)$ = dirac delta distribution, m^{-1}
$\delta_{i,j}$ = Kronecker delta
ϵ = a particle mass, kg
λ = a particle size, m
ρ_s = solid density, taken as 2,500, $kg \cdot m^{-3}$
χ^2 = goodness of fit

Superscripts

A = aggregation
B = breakage

Subscripts

0 = of the zeroth moment
1 = of the first moment
A,B,C = of parameters
b = of breakage
f = of fragments
g = geometric
gv = geometric, volume-based
i,j = of size class i
k = of a time interval
T = of tracer

Other marks

$\overset{+}{}$ = intermediate breakage function
$\hat{}$ = normalized density function
$\tilde{}$ = predicted by simulation
$\bar{}$ = mean, or averaged

Literature Cited

Adetayo, A. A., J. D. Litster, S. E. Pratsinis, and B. J. Ennis, "Population Balance Modelling of Drum Granulation of Materials With Wide Side Distributions," *Power Technol.*, **82**, 37 (1995).

Bramley, A. S., and M. J. Hounslow, "Aggregation during Precipitation from Solution: A Method for Extracting Rates from Experimental Data," *J. Coll. Interf. Sci.*, **183**, 155 (1996).

Eyre, D., R. C. Everson, and Q. P. Campbell, "New Parameterization for a Discrete Batch Grinding Equation," *Powder Technol.*, **98**, 265 (1998).

Hounslow, M. J., R. L. Ryall, and V. R. Marshall, "A Discretized Population Balance for Nucleation, Growth and Aggregation," *AIChE J.*, **34**, 1821 (1988).

Hounslow, M. J., "The Population Balance as a Tool for Understanding Particle Rate Processes," *Kona*, 179 (1998).

Hounslow, M. J., H. S. Mumtaz, A. P. Collier, J. P. Barrick, and A. S. Bramley, "A Micro-Mechanical Model for the Rate of Aggregation during Precipitation from Solution," *Chem. Eng. Sci.*, **56**, 2543 (2001).

Hounslow, M. J., *DPB: A Mathematica Package for Population Balance Calculations*, available on the Web at http://www.shef.ac.uk/uni/projects/ppg/dpb.htm (1999).

Hulburt, H. M., and S. Katz, "Some Problems in Particle Technology: A Statistical Mechanical Formulation," *Chem. Eng. Sci.*, **19**, 555 (1964).

Ilievski, D., and M. J. Hounslow, "Agglomeration During Precipitations: II. Mechanism Deduction from Tracer Data," *AIChE J.*, **41**, 525 (1995).

Muralidar, R., and D. Ramkrishna, "An Inverse Problem in Agglomeration Kinetics," *J. Colloid Interface Sci.*, **112**, 348 (1986).

Pearson, J. M. K., M. J. Hounslow, T. Instone, and P. C. Knight, "Granulation Kinetics: the confounding of particle age and size," *Proc. 3rd Inst. Symp. Part. Tech.*, Brighton U.K. (1998).

Pearson, J. M. K., M. J. Hounslow, and T. Instone, "Tracer Studies of High-Shear Granulation: I. Experimental Results," *AIChE J.*, **47**(9), 1978 (2001).

Press, W. H., S. A. Teukolsky, W. T. Vetterling, and B. P. Flannery, *Numerical Recipes in FORTRAN: The Art of Scientific Computing*, 2nd ed., Cambridge University Press (1992).

Ramkrishna, D., "The Status of Population Balances," *Rev. in Chem. Eng.*, **1**, 49 (1985).
Randolph, A. D., and M. A. Larson, *Theory of Particulate Processes*, 2nd ed., Academic Press, New York (1988).
Sastry, K. V. S., "Similarity Size Distribution of Agglomerates During Their Growth by Coalescence in Granulation or Green Pelletization," *Int. J. Min. Prog.*, **2**, 187 (1975).
Scott, A. C., M. J. Hounslow, and T. Instone, "Direct Evidence of Heterogeneity During High-Shear Granulation," *Powder Technol.*, **113**, 205 (2000).
Smoluchowski, M. V., "Mathematical Theory of the Kinetics of the Coagulation of Colloidal Solutions," *Z. Phys. Chem.*, **92**, 129 (1917).

Appendix A

In this Appendix we show that Eqs. 16 to 19 correctly predict that mass of tracer is conserved.

Aggregation

Conservation of tracer requires

$$\int_0^\infty \overline{B}_1^A(t,v) - \overline{D}_1^A(t,v)dv = 0 \qquad \text{(A1)}$$

Taking the first term in this integral

$$\int_0^\infty \overline{B}_1^A(t,v)dv$$

$$= \int_0^\infty \int_0^v \beta(t,v-\epsilon,\epsilon)n(t,\epsilon)M(t,v-\epsilon)d\epsilon dv$$

$$= -\int_0^\infty \int_v^0 \beta(t,u,v-u)n(t,v-u)M(t,u)dudv$$

$$= \int_0^\infty M(t,u)\int_u^\infty \beta(t,u,v-u)n(t,v-u)dvdu$$

$$= \int_0^\infty M(t,u)\int_0^\infty \beta(t,u,v)n(t,v)dvdu$$

$$= \int_0^\infty \overline{D}_1^A(t,u)du$$

which is the second term, that is, Eq. A1 is proven.

Breakage

Adopting the same approach requires

$$\int_0^\infty \overline{B}_1^B(t,v) - \overline{D}_1^B(t,v)dv = 0 \qquad \text{(A2)}$$

$$\int_0^\infty \overline{B}_1^B(t,v)dv = \int_0^\infty \int_v^\infty S(t,\epsilon)b(v,\epsilon)\frac{v}{\epsilon}M(t,\epsilon)d\epsilon dv$$

$$= \int_0^\infty S(t,\epsilon)M(t,\epsilon)\frac{1}{\epsilon}\int_0^\epsilon vb(v,\epsilon)dvd\epsilon$$

$$\text{but } \int_0^\epsilon vb(v,\epsilon)dv = \epsilon$$

$$= \int_0^\infty S(t,\epsilon)M(t,\epsilon)d\epsilon$$

$$= \int_0^\infty \overline{D}_1^B(t,\epsilon)d\epsilon$$

which once again is the second term, that is, Eq. A2 is also proven.

Appendix B

In this Appendix we show that the DPBE for breakage, Eqs. 25, 31 and 34, *must* conserve granule volume. The requirement for this to be true is

$$\sum_{j\le i}\left(\bar{l}_j^3 b_{j,i}\right) = \bar{l}_i^3$$

or

$$\sum_{j\le i}\left(\left(\frac{\bar{l}_j}{\bar{l}_i}\right)^3 b_{j,i}\right) = 1$$

The lefthand side of this equation is

$$\sum_{j\le i}\left(\left(\frac{\bar{l}_j}{\bar{l}_i}\right)^3 b_{j,i}\right) = \sum_{j<i}\left(\frac{\int_{l_i}^{l_{i+1}}\int_{l_j}^{l_j} x^3 S(t,l)b(x,l)dxdl}{\int_{l_i}^{l_{i+1}} l^3 S(t,l)dl}\right)$$

$$+\frac{\int_{l_i}^{l_{i+1}}\int_{l_j}^{l} x^3 S(t,l)b(x,l)dxdl}{\int_{l_i}^{l_{i+1}} l^3 S(t,l)dl}$$

$$= \frac{\int_{l_i}^{l_{i+1}}\int_{0}^{l} x^3 S(t,l)b(x,l)dxdl}{\int_{l_i}^{l_{i+1}} l^3 S(t,l)dl}$$

$$= \frac{\int_{l_i}^{l_{i+1}} S(t,l)\int_{0}^{l} x^3 b(x,l)dxdl}{\int_{l_i}^{l_{i+1}} l^3 S(t,l)dl}$$

$$= 1$$

as required.

Manuscript received Nov. 23, 1999, and revision received Feb. 12, 2001.